



A 3D perspective for understanding the mechanisms of urban heat island and urban morphology using multi-modal geospatial data and interpretable machine learning[☆]

Ting Han ^a,¹, Chenxi Du ^{a,1}, Yijia Xie ^a, Xinyan Xian ^b, Xinchang Zhang ^{c,d,e}, Bisheng Yang ^f, Yiping Chen ^a,^{*}

^a School of Geospatial Engineering and Science, Sun Yat-Sen University, Zhuhai, 519082, China

^b School of Geographical & Earth Sciences, University of Glasgow, Glasgow, G128QQ, United Kingdom

^c School of Geography and Remote Sensing, Guangzhou University, Guangzhou, 510006, China

^d College of Geography and Remote Sensing Sciences, Xinjiang University, Urumqi, 830046, China

^e Guangdong Urban and Rural Planning and Construction Intelligent Service Engineering Technology Research Center, Guangzhou, 511300, China

^f State Key Laboratory of Information Engineering in Surveying, Mapping and Remote Sensing, Wuhan University, Wuhan, 430079, China

ARTICLE INFO

Keywords:

Urban heat island (UHI)

3D urban morphology

Multi-modal data

LiDAR

LightGBM

Interpretable machine learning

ABSTRACT

The urban heat island (UHI) effect influenced by 3D urban morphology exacerbates urban thermal environments and presents significant challenges to sustainable urban development. While previous studies have emphasized the impact of urban morphology indicators on UHI, fine-scale variations and the intricate relationships between these factors remain underexplored. This study employs LiDAR and geotagged data to obtain nine morphological indicators using the deep learning based semantic segmentation methods. An explainable machine learning framework, specifically an ensemble learning model based on Shapley Additive exPlanations (SHAP), is applied to assess the impact of these indicators and their complex interactions on the thermal environment. Using Austin, Texas as a case study, we present a 3D perspective on the morphology-UHI relationship. The results reveal that urban indicators have more significant impact on UHI, with the sky view factor and impervious surface ratio contributing the most. The influence of urban morphological features on UHI exhibits spatial heterogeneity and boundary effects. For example, building volume initially exacerbates UHI, but once it exceeds a certain threshold, it starts to mitigate the heat island effect. Additionally, the interaction between small buildings and dense road networks intensifies UHI, whereas high-rise buildings can alleviate the effects of extensive urbanization on UHI. These findings offer valuable insights into the driving mechanisms of 2D and 3D urban morphology on UHI and provide guidance for optimizing urban design to reduce the urban heat island effect.

1. Introduction

Urban development has resulted in substantial changes in spatial configurations and morphological patterns of cities, significantly affecting the urban environment and the potential for sustainable ecological systems [1–4]. Driven by urbanization, the phenomenon where urban areas exhibit higher temperatures than their surrounding suburban and rural regions is known as the Urban Heat Island (UHI) [5]. Given the significant implications of UHI on local climate patterns, there has been increasing attention on understanding their mechanisms and

drivers [6–9]. It is crucial to elucidate the driving mechanisms of urban morphology on UHI formation, so as to provide a robust foundation for the development and implementation of effective urban policies and planning strategies.

With the development of remote sensing and geo-spatial technology, remote sensing images have been widely used to develop indicators describing urban morphology for UHI study [10–14]. A series of morphological indicators are calculated from remote sensing images, such as land cover [15,16], landscape patterns [17,18], and built environment [19,20], to construct analysis and prediction models with the

[☆] This work was supported by the National Natural Science Foundation of China under Project 42371343, and Basic and Applied Basic Research Foundation of Guangdong Province with Grant No. 2024A1515010986.

^{*} Corresponding author.

E-mail address: chenyp79@mail.sysu.edu.cn (Y. Chen).

¹ The authors contribute equally to this work.

retrieved land surface temperature (LST). Despite providing a 2D perspective of urban morphology, remote sensing images have limitations in capturing the spatial heterogeneity of 3D urban structures.

Currently, most cities tend to grow vertically during expansion. Understanding the vertical spatial characteristics of cities is beneficial for analyzing the thermal effects of complex built environments. 3D morphology reflects the absorption of thermal energy and its impact on microclimates [21]. With the open availability of various spatial observations and geospatial big data, an increasing number of 3D indicators have been developed as new sources for extracting the 3D built environment [22]. Sky view factor (SVF) [23,24] and green view factor (GVF) [25] from street view images are considered for UHI analysis. More crowdsourced geoinformation data are used to generate the height, volume, and density of buildings, providing insights into cities from a volumetric spatial scale [26,27]. Some studies have extracted urban morphology from both 2D and 3D perspectives to illustrate the relationship between urban morphology and LST [4,28,29]. Despite significant progress in 3D urban morphology, there has been less effort in fine-scale local studies and spatial scale accuracy. A fine-grained understanding of urban buildings and landscape patterns is able to still strengthen the understanding and analysis of urban heat islands. Meanwhile, the impact of 3D morphology has varying impact effects on specific cities, the evaluation with more detailed 3D information need to be explored.

Furthermore, urban systems exhibit considerable complexity, necessitating effective models to accurately measure the relationships between various morphological factors and UHI effects. Spatial regression [30] and geographically weighted regression (GWR) [4] have been employed to address the spatial heterogeneity among factors influencing UHI. However, these models face limitations due to their inability to manage multicollinearity, which impedes the determination of correlations and interactions between factors. To address these challenges, machine learning approaches, such as boosted regression trees [31,32], random forest [33], and XGBoost [29], have been utilized to assess the significance of morphological indicators for UHI. Nonetheless, the black box nature of these machine learning methods often hampers their interpretability, thereby complicating the elucidation of morphological contributions to UHI. Recently, Shapley Additive exPlanations (SHAP) method has attracted widespread attention as an explainable method for machine learning. Inspired by this, we are keen to use the SHAP method to explore the UHI effects of urban morphology.

To this end, we propose a new framework to reveal the divergent mechanisms behind UHI from an urban 3D perspective by incorporating multi-modal geospatial data. Firstly, we utilize our previous works to extract urban entities from point clouds and building footprint from remote sensing images. Moreover, we use geo-tagged data to obtain vector polygons for calibration. Secondly, the extracted urban entities are employed to estimate the urban 2D & 3D morphology indicators within spatial grids. Finally, we use LightGBM model and SHAP method to assess the impact of these indicators and explain their contributions to UHI. Taking central area in Austin, Texas as the study case, the contributions of primary urban morphology indicators affecting UHI are extensively examined and assessed, to further highlight the distinguish the underlying mechanisms of UHI effects. The main contributions of our work are as follows:

- By integrating multi-modal geo-spatial data, we establish a multi-dimensional measurement system of urban morphology;
- We provide fine-grained urban understanding from point clouds to create detailed urban spatial values;
- We explore how 2D & 3D urban morphology impact UHI effect from an urban spatial perspective;
- The results of our study shed light the underlying mechanisms of UHI effect and provide evidence and strategies for UHI mitigation.

2. Study area and data

2.1. Study area

Austin (30°17'N, 98°11'W) is located in central Texas on the eastern edge of the American Southwest² (Fig. 1). It is the capital of Texas and one of the four largest cities in Texas and the 11th largest city in the United States, with a population of over 1 million residents, covering approximately 790 km².³ From 2020 to 2023, Austin's urban population and metropolitan area have experienced sustained growth.

Austin is situated within a hilly terrain, with elevations ranging from 80 to 405 m. The Colorado River traverses the downtown area, contributing to the unique topographical features. The hilly topography creates microclimates within the city, affecting temperature distribution and heat retention. The Colorado River serves as a natural cooling mechanism, providing a comparative baseline for understanding the cooling effects of water bodies.

As the capital of Texas, government entities are concentrated in the downtown area, while high-tech companies and factories are dispersed around the city. This makes Austin's architectural style a blend of metropolitan density and rural sprawl. The city is characterized by a mix of high-rise buildings and suburban neighborhoods, creating a diverse urban landscape. The city is dotted with significant vegetation areas, such as parks and green spaces, which help mitigate the surface temperature increases associated with urban expansion.

The interaction between the geographical features and the building environment offers insights into mitigating UHI effects through strategic urban planning. This unique blend of urban and natural features makes it an intriguing case study for examining the spatial heterogeneity of LST within 3D urban perspective. Austin has become an excellent location for studying 3D urban structure and urban thermal environments.

2.2. Data collection

The point clouds data is derived from geospatial data products provided by the Texas Geographic Information Office,⁴ as part of the Texas Strategic Mapping Program. LiDAR data acquisition is conducted between Jan. 26, 2021, and Mar. 7, 2021, using NAD83 and NAVD88 as horizontal and vertical datum, respectively, with a point density of 12 points per square meter. The data format adheres to LAS 1.4 Format 6,⁵ encompassing Intensity, Return Number, Scanner Channel, Classification, and various other attributes. The data is annotated following the ASPRS ALS classification standard, as detailed in Table 1. The second column lists the ASPRS classification categories, and fourth column reflects the actual classes. We manually adjusted the classification to account for features such as rail and road surface as impervious surfaces as well as extract man-made structures from class 0 in CloudCompare⁶ software. Finally, we use distinct colors to label the corresponding categories for visualizing the results. The remote sensing imagery and geo-tagged data are sourced from Google Earth⁷ and OpenStreetMap.⁸

Land surface temperature (LST) data for the study area is obtained from the Sentinel-3 satellites, including data from both Sentinel-3 A and Sentinel-3B. With an orbital period of approximately one day, the combination of these two satellites provides high-frequency, in-scope data concurrent with the point clouds acquisition period. The Sea and Land Surface Temperature Radiometer (SLSTR) onboard these satellites is equipped with multiple thermal infrared (TIR) channels

² <https://www.austintexas.gov/resident/about-city-austin>

³ <https://demographics-austin.hub.arcgis.com/>

⁴ <https://geographic.texas.gov>

⁵ https://www.asprs.org/wp-content/uploads/2019/07/LAS_1_4_r15.pdf

⁶ <https://cloudcompare.org/>

⁷ <https://earth.google.com/web/>

⁸ <https://www.openstreetmap.org/>

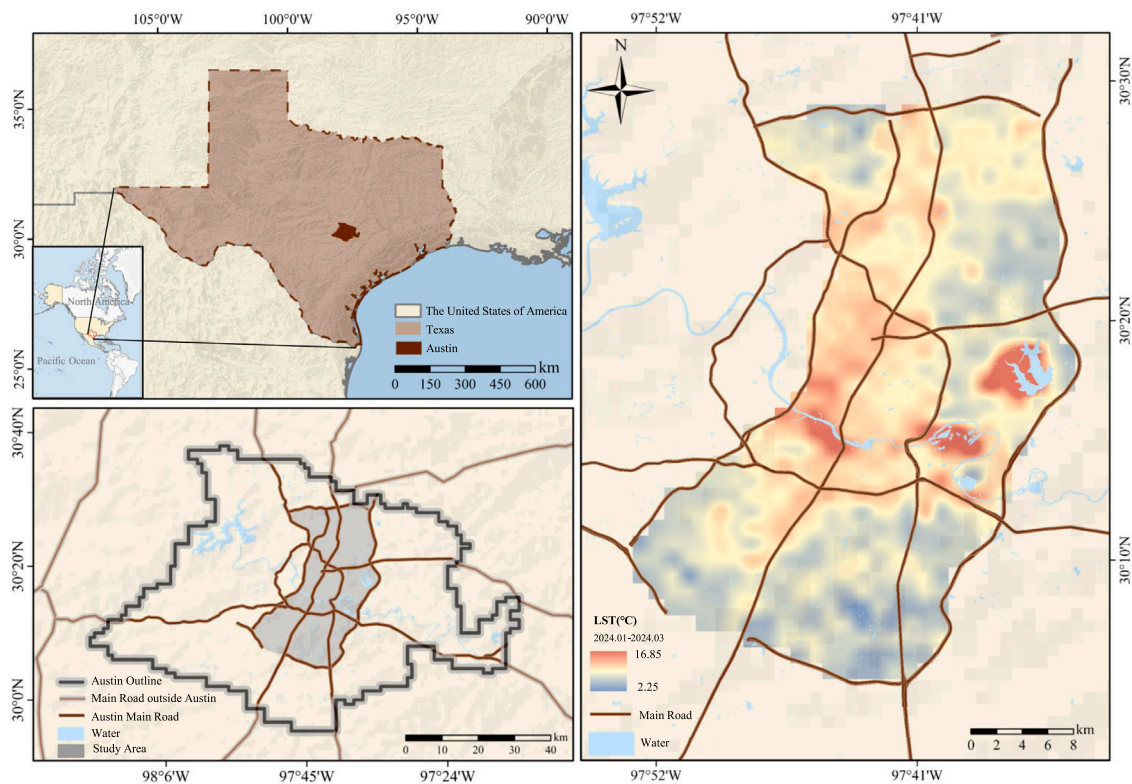


Fig. 1. Location of study area and its land surface temperature pattern. Note that the outline of Austin represents the boundary of the point cloud collection area.

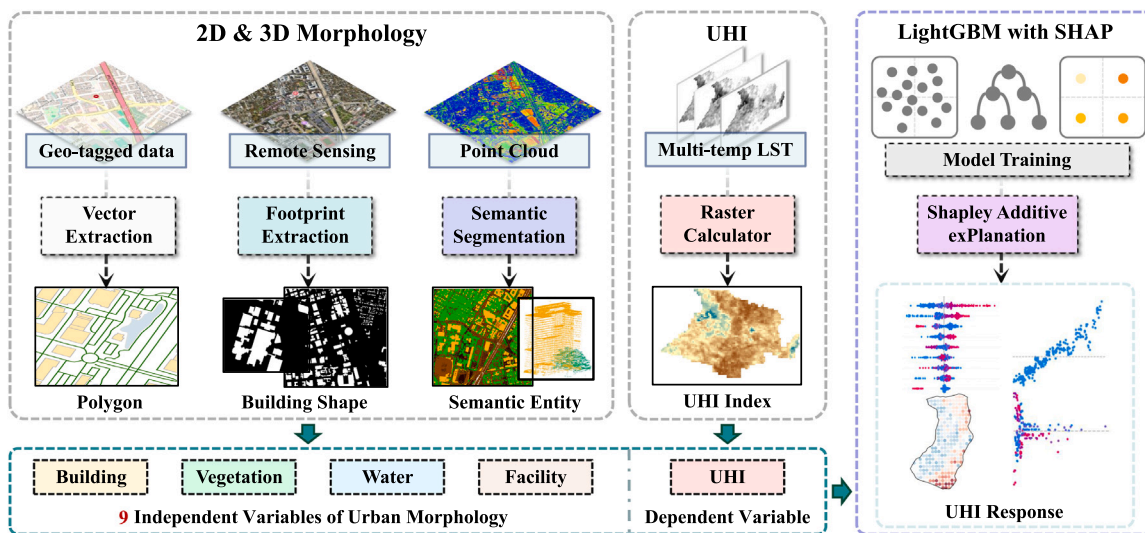


Fig. 2. Framework of investigating the impact of urban morphology on UHI using multi-modal geo-spatial data.

to measure the Earth's surface temperature [34], while visible and near-infrared channels are used to assist in temperature calculations and to provide additional environmental information. The collected information undergoes radiative and atmospheric corrections to ensure high-quality temperature measurements. We filter the data covering the study area through the Copernicus Open Access Hub,⁹ focusing on the period from Jan. 26 to Mar. 4, and exclude any data with large areas of missing values. The final selection includes eight Level-2 data sheets, each with an approximate resolution of 1 km. The average LST

for overlapping areas was calculated to produce the final land surface temperature.

3. Method

To reveal the impact mechanisms and effects of 3D urban morphology on the UHI, we propose a new workflow as illustrated in Fig. 2. Firstly, the proposed deep learning-based semantic segmentation method is utilized to extract major urban entities from large-scale point clouds. Moreover, we integrate remote sensing imagery and geotagged data to jointly extract 2D and 3D urban morphological features. Secondly, multi-temporal LST data are employed to calculate the UHI index. Next, a LightGBM model is constructed with the UHI index as

⁹ <https://www.copernicus.eu/>

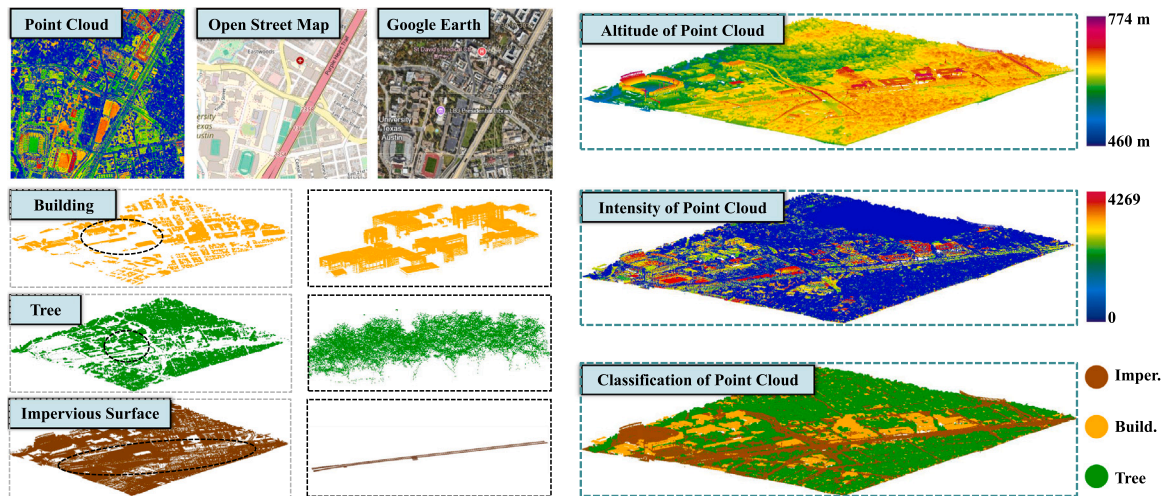


Fig. 3. Examples of point clouds with attributes and corresponding semantic segmentation.

Table 1
Point clouds annotation classification standards and adjustments in our method.

| Value | Class | Select | Actual class | Color |
|--------|---------------------------|--------|--------------------|-------|
| 0 | Created, Never Classified | ✓ | Impervious Surface | ● |
| 1 | Unclassified | — | — | — |
| 2 | Ground | ✓ | Ground | ● |
| 3 | Low Vegetation | ✓ | Vegetation | ● |
| 4 | Medium Vegetation | ✓ | Vegetation | ● |
| 5 | High Vegetation | ✓ | Tree | ● |
| 6 | Building | ✓ | Building | ● |
| 7 | Low Point (Noise) | — | — | — |
| 9 | Water | ✓ | Water | ● |
| 10 | Rail | ✓ | Impervious Surface | ● |
| 11 | Road Surface | ✓ | Impervious Surface | ● |
| 14 | Culverts | ✓ | Impervious Surface | ● |
| 17 | Bridge Decks | ✓ | Impervious Surface | ● |
| 18–255 | ... | — | — | — |

the dependent variable and various urban morphology indicators as independent variables. Finally, the SHAP method is used to interpret the contributions and significance of the these indicators, shedding light on their differences and correlations.

3.1. Urban heat island index

UHI effect refers to the extent to which temperatures in urban areas are higher than those in surrounding rural or natural areas [35]. UHI can be measured using LST data obtained from remote sensing products. The formula of UHI index [36] is as follows:

$$UHI = \frac{T_i - \hat{T}}{\sigma} \quad (1)$$

where T_i and \hat{T} represent the LST value of the current pixel and the mean temperature value of the study area, respectively. σ is the standard deviation of the study area. This approach helps to mitigate the impact of climatic conditions on the UHI, providing a more intuitive and standardized measurement of UHI intensity. The calculations are performed using the ArcMap Raster Calculator.¹⁰

3.2. 2D & 3D urban morphology indicators

We extract urban entities from remote sensing images, point clouds, and geotagged data to obtain 2D and 3D urban morphological indicators. These indicators focus on four key aspects: building, vegetation,

water environment, and urban facilities (as shown in Table 2), with the aim of assessing their impact mechanisms on the UHI effect.

To more effectively extract urban 2D and 3D morphology, we employ multi-modal geospatial data to identify and analyze urban entities. On one hand, point clouds represent the 3D spatial morphology of the city, facilitating the extraction of semantic entities that provide insights into the structural characteristics and distribution of various urban features. On the other hand, geotagged data and remote sensing imagery together enhance the comprehension of 2D features and their spatial distribution, offering a more comprehensive and macro-level perspective on urban environments.

We utilize the proposed ASGFormer [37] to extract urban objects from large-scale urban point clouds. ASGFormer takes point clouds as input and performs semantic segmentation on the point clouds using a Graph Transformer network. Thus, the 3D spatial structure is obtained to characterize 3D features and spatial morphology among different urban semantic categories. Specifically, The input data consists of point cloud coordinates (XYZ) and intensity, which are voxelized using a voxel size of 0.5 m. In total, we obtain 1245 point cloud blocks, among which 245 are randomly selected for training to predict the remaining 1000 unlabeled samples. During training, we use CrossEntropy loss with label smoothing, the AdamW optimizer, and a cosine learning rate decay. The initial learning rate is set to 0.01, and the batch size is 16. The model is trained on an NVIDIA A100 GPU, and the best-performing model on the validation set is used for inference. Finally, semantic segmentation results are mapped back to the original point clouds for subsequent analysis of urban 3D morphological indicators.

The semantic segmentation examples are shown in Fig. 3. As a typical area of Austin, the region near the University of Texas features diverse building types and dense green coverage. We extract buildings, low / medium/high vegetation, impervious surfaces, and some water bodies in the city to calculate subsequent urban 3D morphology indicators. Meanwhile, remote sensing imagery is leveraged to extract building footprints and road networks. The proposed method [14] is capable of adapting to roads and buildings of various sizes, shapes, and densities. Finally, urban entity vectors are derived from geotagged data, such as OSM. These methods information enable the estimation of more accurate, comprehensive, and multidimensional 2D and 3D urban morphology indicators.

Based on the point clouds data format, we divide the remote sensing images, vector maps, and point clouds into identical blocks. Each block is then further divided into a 25 × 25 grid, within which morphological indicators are calculated. First, ground points are interpolated into a DEM for each grid, and the height difference is calculated by subtracting the DEM from the feature points. Next, polygons are extracted from

¹⁰ <https://www.esri.com/zh-cn/arcgis/products/arcgisdesktop/resources>

Table 2

2D and 3D urban morphology indicators in four key aspects, where b, g, t, w, is, r denote the building, ground, tree, water, impervious surface, and road, respectively.

| Aspects | Name | Type | Abbr. | Description | Calculation |
|------------|---------------------------|------|-------|---|----------------------------------|
| Building | Building Total Area | 2D | BTA | Total area of building | $\sum_{i=1}^n A_b^i$ |
| | Average Building Height | 3D | ABH | Average height of building | $\frac{1}{n} \sum_{i=1}^n H_b^i$ |
| | Average Building Volume | 3D | ABV | Average volume of building | $\frac{1}{n} \sum_{i=1}^n V_b^i$ |
| | Building Ratio | 3D | BR | Percentage building footprint points to all ground points | N_{um_b} / N_{um_g} |
| | Sky View Factor | 3D | SVF | Percentage of sky space to total space | V_{sky} / V_{total} |
| Vegetation | Average Tree Height | 3D | ATH | Average height of tree | $\frac{1}{n} \sum_{i=1}^n H_t^i$ |
| Water | Water Area | 3D | WA | Total area of water | $\sum_{i=1}^n A_w^i$ |
| Facility | Density of Road | 2D | DR | Ratio of road length to area | L_r / A_{total} |
| | Impervious Surfaces Ratio | 3D | ISR | Percentage impervious surface points to all ground points | $N_{um_{is}} / N_{um_g}$ |

the building footprints and road networks, and manually adjusted to align with vectors from OSM. Finally, the elevation and polygons are used to calculate the morphological indicators.

Previous studies [4,29,38,39] have shown that the UHI effect is significantly influenced by the 2D and 3D morphology of buildings. To provide a more comprehensive understanding, we incorporate a set of urban morphological indicators categorized into four key aspects: buildings, vegetation, water, and facilities. These indicators jointly describe both horizontal and vertical spatial features and facilitate an in-depth analysis of their relationship with the UHI effect from a 3D spatial perspective. Moreover, we utilize a large language model (LLM) for a preliminary interpretation of these indicators [40], which supports the subsequent quantitative analysis.

3.3. LightGBM regression model

LightGBM is a highly efficient algorithm based on Gradient Boosting Decision Trees (GBDT), specifically designed to handle high-dimensional features and large-scale datasets [41,42]. It operates by iteratively building an ensemble of weak predictive models, such as decision trees, and combining their predictions to create a robust final model. Unlike traditional GBDT implementations, LightGBM uses a leaf-wise growth strategy with depth constraints, the algorithm splits only the leaf node with the highest information gain at each iteration. This approach reduces the number of splits, optimizing both memory usage and computational efficiency. Additionally, it restricts the depth of decision trees to prevent overfitting. Consequently, LightGBM offers faster training speeds, lower memory consumption, higher accuracy, and improved scalability when working with large datasets [41].

In this study, LightGBM is executed with UHI as the dependent variable, and nine urban morphology as independent variables. Thus, morphological indicators are used as input features for the LightGBM model to predict UHI. The dataset from the study area is split into training and validation sets with a 7:3 ratio. The grid search is employed to optimize the model parameters. This modeling process is implemented using Python 3.7.16¹¹ with the sklearn¹² and lightgbm¹³ libraries. Subsequently, the coefficient of determination (R^2) and root mean square error (RMSE) are applied to measure the model accuracy.

3.4. SHAP method

To address the black box issue commonly associated with machine learning models, we employ the SHAP method [43] to interpret the prediction process of the LightGBM model [44]. SHAP is a local interpretation method based on cooperative game theory's Shapley values. It constructs an additive explanation model to quantify the contribution

of each feature to the model's output for each individual sample. The formula for SHAP is as follows:

$$\widehat{UHI} = UHI_{base} + \sum_{i=1}^N shap_i \quad (2)$$

where UHI_{base} represents the baseline value, which is the mean UHI value across the study area. N and $shap_i$ denote the number of features and the contribution of feature i of all sample points to the predicted UHI, respectively. The relative contribution weight $W(i)$ of feature i to UHI is calculated as follow:

$$W(i) = \frac{|shap_i|}{\sum_{i=1}^N |shap_i|} \quad (3)$$

where $|shap_i|$ denotes the mean |SHAP| value for feature i .

In UHI research, urban morphological features do not function in isolation. The SHAP method also enables the calculation of SHAP_{interaction_values}, which provide insights into the interaction effects between pairs of features. For any given feature, its SHAP value is the sum of its main effect and its interaction effects with all other features. A more detailed explanation can be found in [43].

4. Results

4.1. Spatial distribution of UHI and urban morphology indicators

Before conducting the LightGBM modeling, the selected nine 2D & 3D urban morphology indicators and calculated UHI index are statistically evaluated in terms of distributions and intensity, as shown in Fig. 4(a). Both ABV and ABH did not exhibit distribution characteristics, whereas BTA, BR, ISR, and DR display similar spatial distribution characteristics. Moreover, water bodies and vegetation also exhibit relatively distinct distribution patterns.

In the western part of the study area, building coverage is highly concentrated, as evidenced by the high BTA, BR, and DR. This is consistent with the population distribution in the Austin from U.S. Census.¹⁴ Since impervious surfaces are mainly concentrated in roads and urban facilities, their spatial distribution is similar to that of roads and buildings. BR and SVF exhibit an inverse relationship, meaning that in areas with high building density, urban morphology tends to be compact, thereby reducing the SVF. Due to the Colorado River running through Austin, the distribution of major water bodies aligns with the river basin, showing a normal distribution. Adequate water systems help mitigate the UHI effect, with features such as streams playing a cooling role, while plants growing along the banks provide shade and absorb moisture. Austin is a city with dense vegetation, and most areas have high vegetation coverage. The southwestern part of the study area is hilly, and the presence of a Wildflower Center contributes to the higher vegetation rate in this region.

The average temperature of Austin is around 20 °C, which matches the value we calculated. The calculated UHI values are shown in Fig.

¹¹ <https://www.python.org/>

¹² <https://scikit-learn.org/stable/index.html>

¹³ <https://lightgbm.readthedocs.io/en/latest/Python-Intro.html>

¹⁴ <https://demographics-austin.hub.arcgis.com>

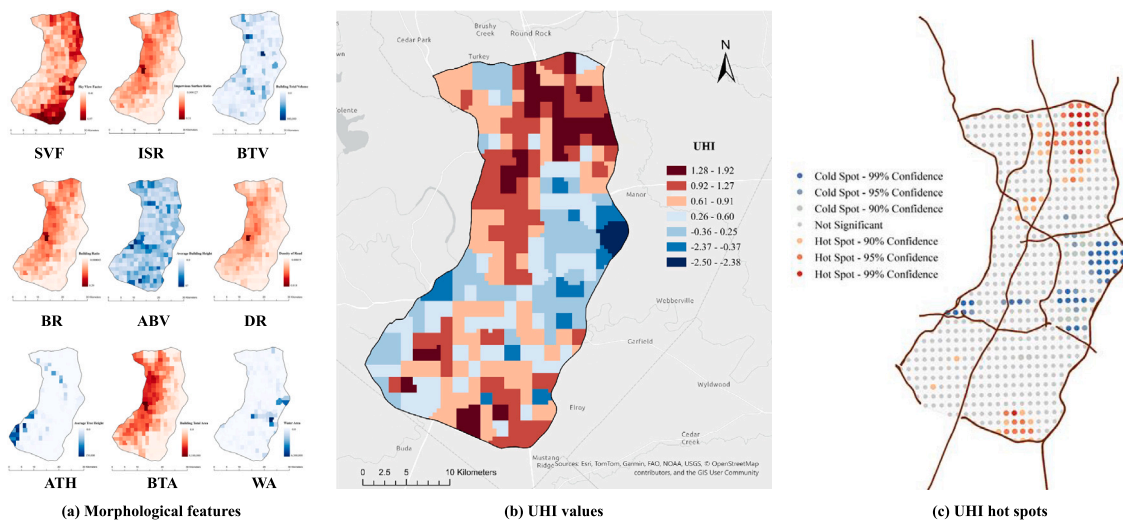


Fig. 4. The selected 2D & 3D urban morphology components and UHI index investigated in our study, where (a) denotes the distribution of urban morphology indicators, (b) represents the UHI values in the center of Austin, and (c) shows the UHI hot spots.

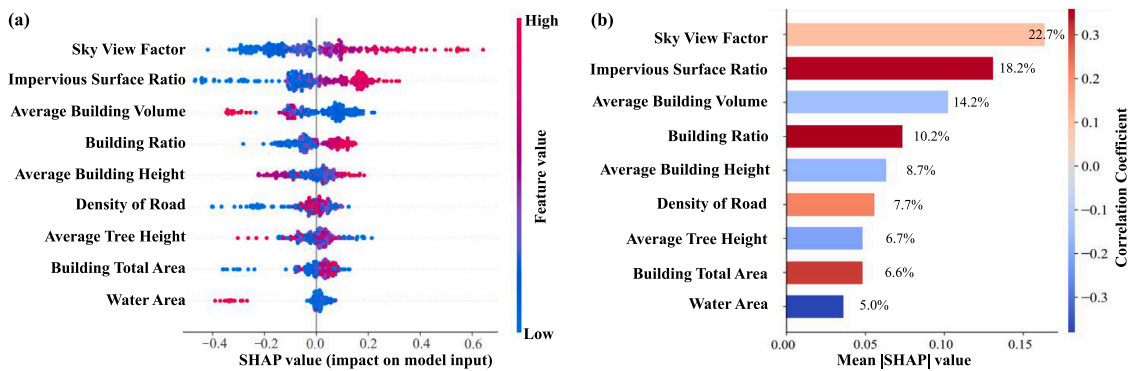


Fig. 5. SHAP summary plot of urban morphological features on LightGBM model output (a). UHI response to urban morphological features: Feature importance plot with bar colors representing Pearson correlation coefficients, the numbers on the right side of the bars represent the relative contribution weights of the corresponding features to UHI (b).

4(b). For a semi-arid region in the Austin, heat stress is a health issue that must be addressed. Our results shows that UHI effect has a high correlation with urban morphology. The spatial characteristics of the UHI are shown in Fig. 4(c). The northern and southern parts of the study area are high-value UHI clusters, while the central-eastern part is a low-value cluster. Areas with dense buildings and road networks exhibit significantly higher temperatures. On one hand, high urban density promotes more concentrated activities such as population, industry, and transportation, leading to an increase in total carbon emissions. On the other hand, the rapid development of Austin has resulted in significant traffic congestion, making transportation the second-largest source of carbon emissions in the city. Meanwhile, river basins and regions with high vegetation coverage play a clear cooling role. The evaporation of moisture and the healthy growth of vegetation have become the city’s natural air conditioning.

4.2. Response of UHI to urban morphological indicators

A LightGBM model is constructed to fit the UHI effect using urban morphological indicators ($R^2 = 0.62$, $RMSE = 0.45$), and SHAP method is subsequently applied to interpret the internal processes of model. By aggregating SHAP values for each indicator and calculating Pearson correlation coefficients, we assess the relative importance and direction of influence of urban morphology on UHI. We find that 3D urban morphology factors play a more significant role in influencing UHI effect, with SVF, ISR, and ABV having the most substantial impact,

as shown in Fig. 5. Their relative contribution weights are 22.7%, 18.2%, 14.2%, respectively. Specifically, SVF ($r = 0.10$) and ISR ($r = 0.35$) are positively correlated with UHI, while building volume ($r = -0.14$) and building height ($r = -0.37$) show a negative correlation in Fig. 5. The feature importance analysis indicates that the 3D building metrics (ABH, ABV, BR, SVF) ranks among the top five in terms of their contribution.

The dependencies between each feature value and its corresponding SHAP value for all samples are plotted to explore how these features influence UHI, as shown in Fig. 6. The dashed lines differentiate the positive and negative effects of urban morphological features on UHI. Threshold effects are observed in the influence of these features on UHI. For instance, when the building volume is below approximately 100,000, it has a positive effect on UHI, intensifying the heat island effect. However, when building volume exceeds threshold, its effect shifts to mitigating UHI. Similarly, the thresholds for SVF, ISR, and BR are identified at 0.7, 0.1, and 0.1, respectively. Beyond these thresholds, their influence transitions from mitigating to promoting UHI. The impact of road density exhibits an inverted U-shape, where both extremely high and low level of road density help alleviate UHI.

Besides the statistic and importance of urban morphology, it is imperative to investigate the spatial distribution of the positive and negative impact of different urban morphology indicators on the UHI effect. The spatial distribution of SHAP values provides localized insights into the impact of urban morphological metrics on UHI, as shown in Fig. 7. The color gradient from red to blue represents the transition

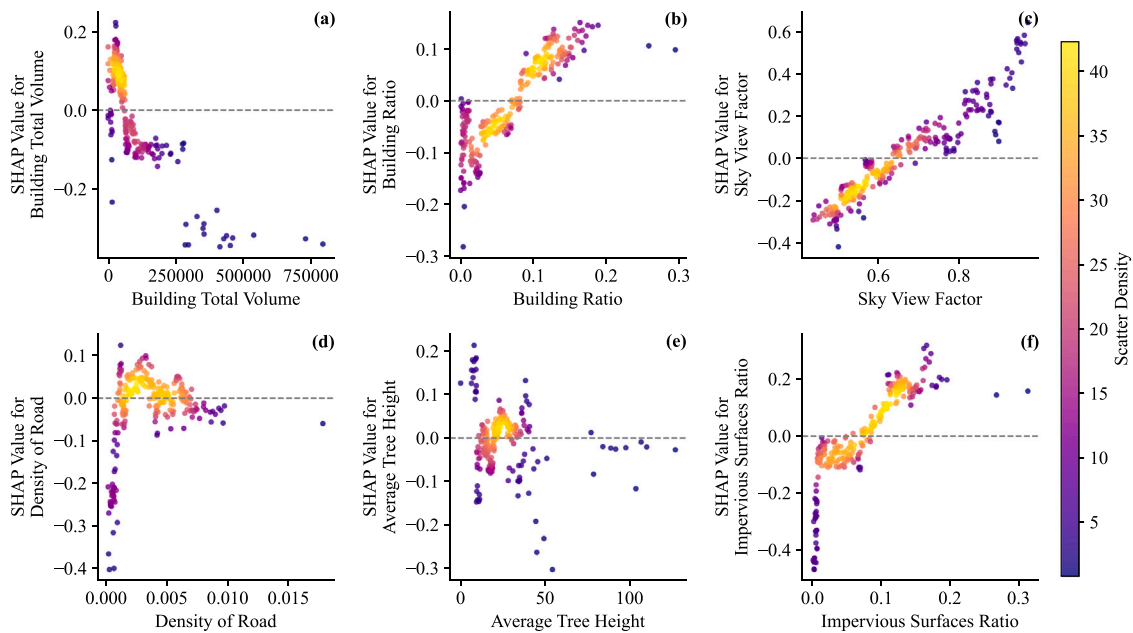


Fig. 6. SHAP dependence plots for urban morphology features.

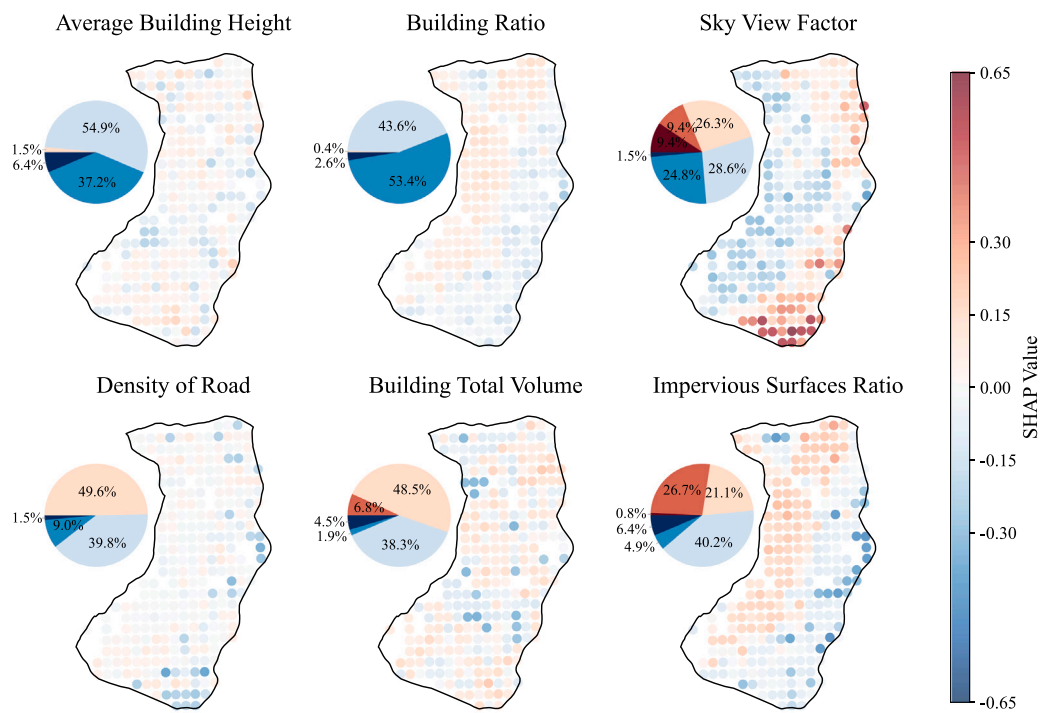


Fig. 7. Spatial distribution of SHAP values for urban morphology features.

from positive to negative impacts, where a larger extent of red indicates a stronger positive contribution to UHI, and vice versa. The spatial heterogeneity observed across the study area highlights the variability in these effects.

SVF exhibits significant spatial clustering and has the strongest influence among all metrics, with 45.1% of the area showing $|\text{SHAP}| > 0.15$. Notably, 9.4% of the area has SHAP values ranging from 0.3 to 0.65, primarily concentrated in the southern part of the region, indicating that SVF strongly amplifies UHI intensity there. In contrast, ISR displays an opposite spatial pattern to SVF and also has a relatively

strong impact, with 39.7% of the area showing $|\text{SHAP}| > 0.15$. The impact of DR on UHI is slightly more negative than positive. Specifically, 49.6% of the area has SHAP values between 0 and 0.15, while 39.8% falls within the range of $-0.15 < \text{SHAP} < 0$, and 10.5% of the area has SHAP values below -0.15 . The strongest negative effects are mainly concentrated in the southeastern part of the region, as well as in a small portion of the eastern area.

It demonstrate different spatial patterns can also be observed within the same category. Although SVF and ISR are widely used for measuring the compactness of the city, it is hard to tell which is a better

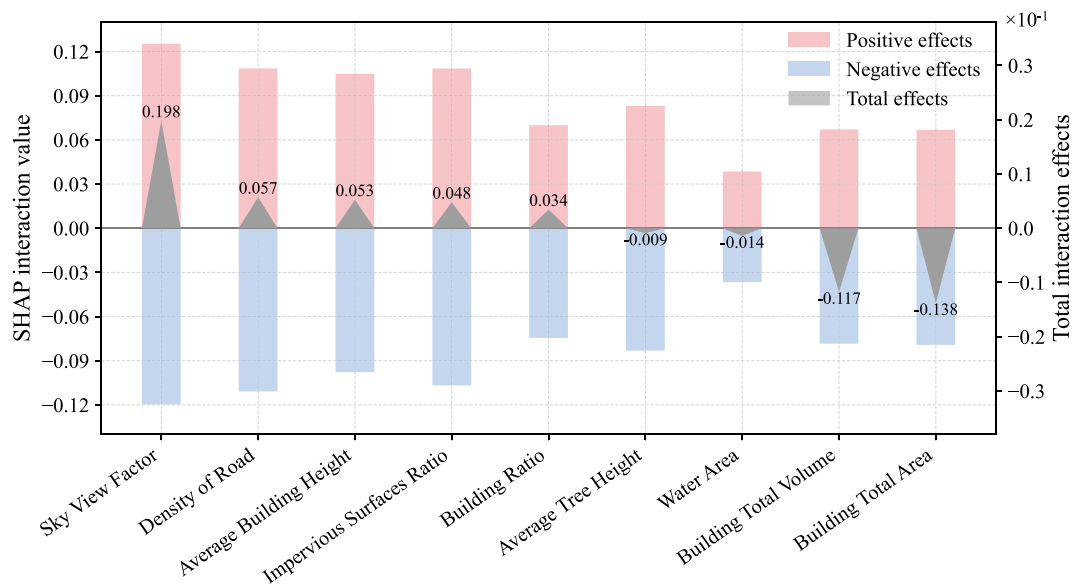


Fig. 8. The summary of the interactions between a single feature and all other features except itself.

indicator. Thus, we need to combine these indicators to obtain a better understanding about how urban morphology affect the UHI.

4.3. Influence of feature interactions on UHI

SHAP interaction values provide insights into how interactions between urban morphological features impact UHI. Fig. 8 summarizes the interactions between each feature and all other features. It is found that the interactions between urban morphology features can either exacerbate or alleviate UHI, depending on the specific conditions. Positive and negative interaction effects of each feature can partially offset each other. From a global perspective, building volume tends to mitigate UHI when interacting with other features, while SVF and DR tend to intensify UHI through their interactions.

Examining the interactions between ABV, ABH, and other features, we observe that when the ABV is below 100,000, interactions with DR tend to exacerbate UHI. However, when the ABV exceeds 100,000, interactions with DR help mitigate UHI. Similarly, when ABV is low, low SVF and tall trees helps to mitigate UHI. In contrast, with higher building volume, dense vegetation can actually intensify UHI (Fig. 9(a-c)). Additionally, higher BR, DR, and ISR signify a more developed urban environment. In such conditions, interactions with tall buildings can contribute to alleviating UHI (Fig. 9(d-f)).

5. Discussion

5.1. Impact of urban morphological features on UHI

This study utilizes the LightGBM-SHAP framework to examine the impact of urban morphological features on UHI effects. Our findings indicate that, among various urban morphological factors, 3D building metrics have a more significant impact on UHI compared to other factors. This conclusion aligns with prior research conducted in different urban contexts [45]. Additionally, the analysis of the relationship between SHAP values and urban morphological features reveals both nonlinear and threshold effects of these features on UHI.

Our results build upon the previously established positive correlation between SVF and UHI [23,46]. Specifically, we find that when SVF is below 0.7, it mitigates UHI by enhancing street ventilation [47]. However, when SVF exceeds this threshold, the increased openness leads to greater surface exposure to solar radiation, resulting in higher temperatures [48]. It is important to recognize that the impact of

SVF on UHI can vary significantly across different spatial scales. This variation may be influenced by factors such as the study area, block layout, and building density. For instance, [49] reported a negative correlation between LST and SVF at the block scale (i.e., irregular grid). These findings highlight the importance of considering scale effects in future research.

Similarly, the influence of ISR on UHI also exhibits a threshold effect. When ISR is below 0.1, the evaporation effect on urban surfaces significantly reduces surface temperatures. However, as ISR increases, the cooling effect of evaporation diminishes, and impervious surfaces begin to absorb and store more heat, thereby exacerbating UHI. This occurs because impervious surfaces alter the latent and sensible heat fluxes within the urban boundary layer and surface layer, with increased impervious surfaces disrupting natural heat exchange [50, 51].

Building volume also exhibits a distinct threshold effect on UHI. When building volume is less than 100,000, UHI is intensified due to larger exposed areas and localized heat accumulation. However, once the building volume exceeds this threshold, the combined effects of shading from compact, tall buildings [31] and the canyon effect created by ventilation corridors [52] help to mitigate UHI. Additionally, road density follows an inverted 'U'-shape in its impact. While higher density facilitates ventilation and heat exchange, thereby reducing UHI. Excessive road density leads to increased heat buildup between buildings and elevated traffic heat emissions, which in turn exacerbate UHI effects [53]. At the same time, in high-tech industrial areas, the increased construction of light rail has significantly reduced urban transportation carbon emissions, compared to automobile traffic.

5.2. Unraveling complex interactions of urban morphological features on UHI effects

Firstly, the intricate interplay between urban morphological features and their impact on UHI effects is analyzed using SHAP interaction values. When building volume is relatively low, its interaction with a dense road network exacerbates UHI, as the limited air circulation caused by dense roads can lead to heat accumulation. However, as building volume increases, the ventilation effect of the road network becomes more pronounced, helping to mitigate UHI. This phenomenon can be attributed to the urban canyon effect, where dense arrangement of buildings and roads may create effective ventilation corridors under certain conditions, thereby reducing local temperatures [54].

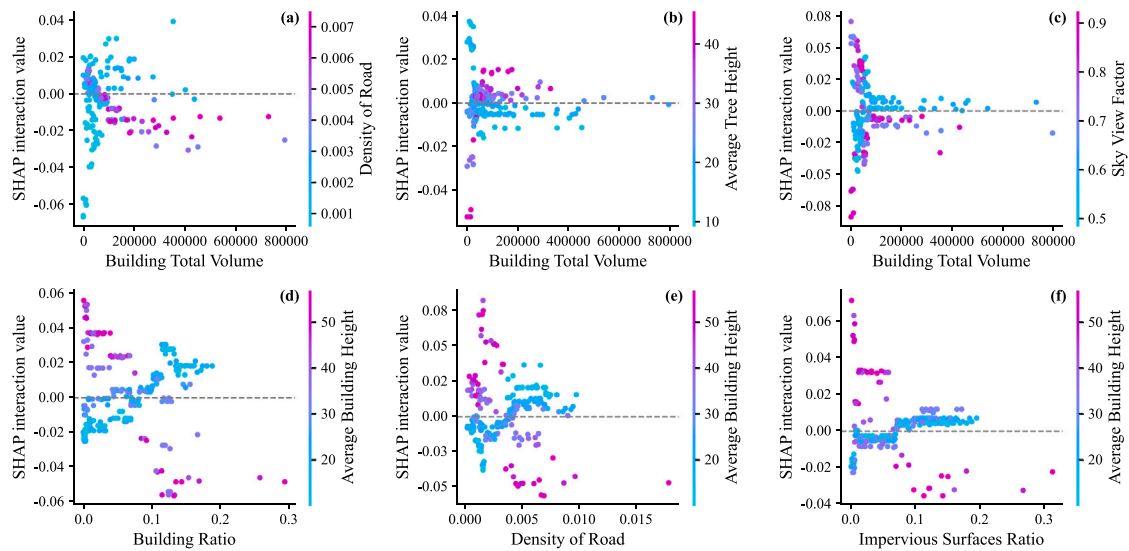


Fig. 9. SHAP interaction plots for urban morphology features.

Secondly, the interaction between building volume and vegetation cover also shows significant effects. When building volume is small and SVF is low, dense tree coverage can effectively blocks solar radiation, thereby alleviating UHI effects [55]. Conversely, as building volume increases, reduced sky visibility can contribute to heat retention at the surface, exacerbating UHI [56].

Moreover, the interaction between building height and road density exhibits complex effects. Research indicates that increased building height reduces local heat accumulation by casting shadows and enhancing air circulation, especially in high-density areas where this cooling effect on UHI is more pronounced. Therefore, in regions with high building and road densities, tall buildings often help mitigate UHI. However, when road density becomes excessively high, heat from traffic emissions and road surfaces accumulates locally, counteracting the shading effect of buildings and leading to further intensification of UHI [54,57,58].

Finally, a high proportion of impervious surfaces, combined with a dense road network and tall buildings, can help mitigate UHI by enhancing wind circulation and reducing solar radiation exposure [59]. These complex interactions highlight the dynamic and multi-dimensional nature of UHI mechanisms across various urban morphology combinations. They emphasize the importance of considering the combined effects of urban morphology in city planning and design to more effectively address and mitigate UHI effect.

5.3. Limitations

There are still some limitations in this study. Firstly, we focus on cold months (Jan. to Mar.), hot and moderate months should be further investigated. A single-season temperature may lead to a biased analysis of the impact mechanism. In future work, we plan to incorporate multi-seasonal land surface temperature data to investigate the temporal dynamics of UHI patterns across different climate regimes.

Secondly, the UHI effect at the block scale, combined with building functions, needs further exploration to provide insights into urban functional zones.

Next, proportions of different buildings, such as low-rise, mid-rise, and high-rise buildings, are worth further discussion. The different temperature effects in the vertical direction are meaningful for urban studies.

Finally, the distance or proximity of other infrastructures to each block could be regarded as a key variable, which can be worth further investigating to understand the cooling effects of infrastructures spilling over the block boundary.

6. Conclusion

This paper integrates 2D & 3D urban morphology indicators and utilizes LightGBM-SHAP framework to investigate the impacts and driving mechanisms related to the UHI effect by using multi-modal geo-spatial data. Firstly, we employ deep learning based semantic segmentation methods to extract urban entities from LiDAR and remote sensing imagery, and also obtain vector polygons from geo-tagged data. Next, we estimate urban 2D & 3D morphological indicators and select nine variables from the candidate indicators for subsequent modeling based on their correlation coefficients. Lastly, LightGBM-SHAP method is used to analysis the impact of those indicators on UHI and explain their contributions. We provide precise spatial measurements, detailed and high-confidence urban morphology, along with a comprehensive analysis of impact mechanisms and driving factors.

Taking Austin, Texas as the study case, the main conclusions are as follows:

- Urban indicators have a significant impact on UHI effect. Urban morphology features such as SVF and ISR contribute to increasing UHI, while building volume and height help reduce it;
- Urban morphological features exhibit threshold or boundary effects on UHI, where their influence shifts between intensifying and mitigating UHI beyond certain critical points. For instance, building volume may initially exacerbate UHI, but once it exceeds a certain threshold, it begins to alleviate the heat island effect. Similarly, indicators like SVF and ISR also show threshold effects. Spatially, these effects vary across different regions, with densely built areas experiencing stronger UHI effects, while regions with more vegetation or water bodies show cooling effects, emphasizing the regional variability in how urban morphology impacts UHI;
- Interactions between urban morphological features can either intensify or mitigate UHI depending on their combinations. For example, the interaction between lower building volume and road density typically exacerbates UHI, while higher building volume tends to alleviate it. Additionally, interactions between building height and other features, such as higher ISR representing advanced urban development, can also help mitigate UHI in certain cases.

The above findings indicate that integrating urban morphology extracted from multi-modal geo-spatial data with the LightGBM-SHAP framework is an effective and practical workflow for assessing UHI

effects, providing valuable insights to inform decision-making in urban planning and facilitate sustainable urban development.

Despite the achievement in our study, there is still room to improve the understanding of the relationship between other factors of urbanization and UHI, as well as in more rational spatial delineation. In the future, we will explore more comprehensive spatiotemporal variation indicators based on socio-economic metrics to better elucidate the underlying mechanisms of UHI.

CRedit authorship contribution statement

Ting Han: Writing – review & editing, Writing – original draft, Visualization, Methodology, Investigation, Data curation, Conceptualization. **Chenxi Du:** Writing – original draft, Visualization, Methodology, Formal analysis, Conceptualization. **Yijia Xie:** Writing – original draft, Visualization, Methodology, Investigation. **Xinyan Xian:** Visualization, Methodology, Conceptualization. **Xinchang Zhang:** Supervision, Resources, Investigation. **Bisheng Yang:** Validation, Supervision, Investigation, Formal analysis. **Yiping Chen:** Writing – review & editing, Supervision, Resources, Methodology, Funding acquisition, Conceptualization.

Declaration of competing interest

The authors declare that they have no known competing financial interests or personal relationships that could have appeared to influence the work reported in this paper.

Acknowledgments

The authors would like to thank the National Natural Science Foundation of China under Project 42371343, and Basic and Applied Basic Research Foundation of Guangdong Province with grant No. 2024A1515010986. We sincerely thank Professor Tianxing Chu from the Department of Computer Science at Texas A&M University for his thorough review of our work and his invaluable contributions to validating our results.

We also appreciate the valuable comments and constructive suggestions from the anonymous reviewers that helped improve the manuscript.

Data availability

Data will be made available on request.

References

- N.B. Grimm, S.H. Faeth, N.E. Golubiewski, C.L. Redman, J. Wu, X. Bai, J.M. Briggs, Global change and the ecology of cities, *Science* 319 (5864) (2008) 756–760.
- C. Chen, T. Park, X. Wang, S. Piao, B. Xu, R.K. Chaturvedi, R. Fuchs, V. Brovkin, P. Ciais, R. Fensholt, et al., China and India lead in greening of the world through land-use management, *Nat. Sustain.* 2 (2) (2019) 122–129.
- K. Winkler, R. Fuchs, M. Rounsevell, M. Herold, Global land use changes are four times greater than previously estimated, *Nat. Commun.* 12 (1) (2021) 2501.
- Y. Wang, Z. He, W. Zhai, S. Wang, C. Zhao, How do the 3D urban morphological characteristics spatiotemporally affect the urban thermal environment? A case study of San Antonio, *Build. Environ.* 261 (2024) 111738.
- S. Peng, S. Piao, P. Ciais, P. Friedlingstein, C. Ottle, F.M. Bréon, H. Nan, L. Zhou, R.B. Myneni, Surface urban heat island across 419 global big cities, *Environ. Sci. Technol.* 46 (2) (2012) 696–703.
- T.R. Oke, City size and the urban heat island, *Atmos. Environ.* (1967) 7 (8) (1973) 769–779.
- N. Debbage, J.M. Shepherd, The urban heat island effect and city contiguity, *Comput. Environ. Urban Syst.* 54 (2015) 181–194.
- D. Xu, Y. Wang, D. Zhou, Y. Wang, Q. Zhang, Y. Yang, Influences of urban spatial factors on surface urban heat island effect and its spatial heterogeneity: A case study of Xi'an, *Build. Environ.* 248 (2024) 111072.
- H. Zhao, Y. Fang, X. Xu, Quantifying morphology evolutions of urban heat islands and assessing their heat exposure in a metropolis, *Sustain. Cities Soc.* 102 (2024) 105244.
- N. Kikon, P. Singh, S.K. Singh, A. Vyas, Assessment of urban heat islands (UHI) of Noida City, India using multi-temporal satellite data, *Sustain. Cities Soc.* 22 (2016) 19–28.
- K. Deilami, M. Kamruzzaman, Y. Liu, Urban heat island effect: A systematic review of spatio-temporal factors, data, methods, and mitigation measures, *Int. J. Appl. Earth Obs. Geoinf.* 67 (2018) 30–42.
- F. Biljecki, Y.S. Chow, Global building morphology indicators, *Comput. Environ. Urban Syst.* 95 (2022) 101809.
- G. Xian, H. Shi, Q. Zhou, R. Auch, K. Gallo, Z. Wu, M. Kolian, Monitoring and characterizing multi-decadal variations of urban thermal condition using time-series thermal remote sensing and dynamic land cover data, *Remote Sens. Environ.* 269 (2022) 112803.
- X. Xie, T. Han, Y. Du, Y. Chen, Incorporating building information into road extraction from remote sensing images, in: *IGARSS 2024-2024 IEEE International Geoscience and Remote Sensing Symposium*, IEEE, 2024, pp. 8442–8445.
- G. Xian, H. Shi, R. Auch, K. Gallo, Q. Zhou, Z. Wu, M. Kolian, The effects of urban land cover dynamics on urban heat island intensity and temporal trends, *GIScience & Remote. Sens.* 58 (4) (2021) 501–515.
- H. Chen, Q. Deng, Z. Zhou, Z. Ren, X. Shan, Influence of land cover change on spatio-temporal distribution of urban heat island—a case in wuhan main urban area, *Sustain. Cities Soc.* 79 (2022) 103715.
- C. Shen, H. Hou, Y. Zheng, Y. Murayama, R. Wang, T. Hu, Prediction of the future urban heat island intensity and distribution based on landscape composition and configuration: A case study in Hangzhou, *Sustain. Cities Soc.* 83 (2022) 103992.
- H. Zhang, M.y. Kang, Z.r. Guan, R. Zhou, A.I. Zhao, W.j. Wu, H.r. Yang, Assessing the role of urban green infrastructure in mitigating summertime urban heat island (UHI) effect in Metropolitan Shanghai, China, *Sustain. Cities Soc.* (2024) 105605.
- J. Yang, Y. Yang, D. Sun, C. Jin, X. Xiao, Influence of urban morphological characteristics on thermal environment, *Sustain. Cities Soc.* 72 (2021) 103045.
- L. Zhou, F. Hu, B. Wang, C. Wei, D. Sun, S. Wang, Relationship between urban landscape structure and land surface temperature: Spatial hierarchy and interaction effects, *Sustain. Cities Soc.* 80 (2022) 103795.
- Y. Li, S. Schubert, J.P. Kropp, D. Rybski, On the influence of density and morphology on the Urban Heat Island intensity, *Nat. Commun.* 11 (1) (2020) 2647.
- Y. Shen, W. Kong, F. Fei, X. Chen, Y. Xu, C. Huang, J. Yao, Stereoscopic urban morphology metrics enhance the nonlinear scale heterogeneity modeling of UHI with explainable AI, *Urban Clim.* 56 (2024) 102006.
- J. Kim, D.K. Lee, R.D. Brown, S. Kim, J.H. Kim, S. Sung, The effect of extremely low sky view factor on land surface temperatures in urban residential areas, *Sustain. Cities Soc.* 80 (2022) 103799.
- Y.-C. Chiang, H.-H. Liu, D. Li, L.-C. Ho, Quantification through deep learning of sky view factor and greenery on urban streets during hot and cool seasons, *Landsc. Urban Plan.* 232 (2023) 104679.
- D.E. Okumus, F. Terzi, Evaluating the role of urban fabric on surface urban heat island: The case of Istanbul, *Sustain. Cities Soc.* 73 (2021) 103128.
- Y. Chen, B. Shan, X. Yu, Study on the spatial heterogeneity of urban heat islands and influencing factors, *Build. Environ.* 208 (2022) 108604.
- W.B. Wu, Z.W. Yu, J. Ma, B. Zhao, Quantifying the influence of 2D and 3D urban morphology on the thermal environment across climatic zones, *Landsc. Urban Plan.* 226 (2022) 104499.
- X. Huang, Y. Wang, Investigating the effects of 3D urban morphology on the surface urban heat island effect in urban functional zones by using high-resolution remote sensing data: A case study of Wuhan, Central China, *ISPRS J. Photogramm. Remote Sens.* 152 (2019) 119–131.
- A. Lin, H. Wu, W. Luo, K. Fan, H. Liu, How does urban heat island differ across urban functional zones? Insights from 2D/3D urban morphology using geospatial big data, *Urban Clim.* 53 (2024) 101787.
- Z. Xu, Z. Cai, S. Su, M. Kang, Y. Ge, Unraveling the association between the urban polycentric structure and urban surface thermal environment in urbanizing China, *Sustain. Cities Soc.* 76 (2022) 103490.
- P. Zeng, F. Sun, Y. Liu, T. Tian, J. Wu, Q. Dong, S. Peng, Y. Che, The influence of the landscape pattern on the urban land surface temperature varies with the ratio of land components: Insights from 2D/3D building/vegetation metrics, *Sustain. Cities Soc.* 78 (2022) 103599.
- D. Han, H. An, F. Wang, X. Xu, Z. Qiao, M. Wang, X. Sui, S. Liang, X. Hou, H. Cai, et al., Understanding seasonal contributions of urban morphology to thermal environment based on boosted regression tree approach, *Build. Environ.* 226 (2022) 109770.
- Y. Gao, J. Zhao, L. Han, Quantifying the nonlinear relationship between block morphology and the surrounding thermal environment using random forest method, *Sustain. Cities Soc.* 91 (2023) 104443.
- P. Coppo, B. Ricciarelli, F. Brandani, J. Delderfield, M. Ferlet, C. Mutlow, G. Munro, T. Nightingale, D. Smith, S. Bianchi, et al., SLSTR: a high accuracy dual scan temperature radiometer for sea and land surface monitoring from space, *J. Modern Opt.* 57 (18) (2010) 1815–1830.

- [35] S.W. Kim, R.D. Brown, Urban heat island (UHI) intensity and magnitude estimations: A systematic literature review, *Sci. Total Environ.* 779 (2021) 146389.
- [36] A.A. Kafy, A. Al Rakib, K.S. Akter, D.M.A. Jahir, M.S. Sikdar, T.J. Ashrafi, S. Mallik, M.M. Rahman, et al., Assessing and predicting land use/land cover, land surface temperature and urban thermal field variance index using Landsat imagery for Dhaka Metropolitan area, *Environ. Challenges* 4 (2021) 100192.
- [37] T. Han, Y. Chen, J. Ma, X. Liu, W. Zhang, X. Zhang, H. Wang, Point cloud semantic segmentation with adaptive spatial structure graph transformer, *Int. J. Appl. Earth Obs. Geoinf.* 133 (2024) 104105.
- [38] D. Han, H. An, H. Cai, F. Wang, X. Xu, Z. Qiao, K. Jia, Z. Sun, Y. An, How do 2D/3D urban landscapes impact diurnal land surface temperature: Insights from block scale and machine learning algorithms, *Sustain. Cities Soc.* 99 (2023) 104933.
- [39] L. Shao, W. Liao, P. Li, M. Luo, X. Xiong, X. Liu, Drivers of global surface urban heat islands: Surface property, climate background, and 2D/3D urban morphologies, *Build. Environ.* 242 (2023) 110581.
- [40] Y. Chen, S. Zhang, T. Han, Y. Du, W. Zhang, J. Li, Chat3D: Interactive understanding 3D scene-level point clouds by chatting with foundation model for urban ecological construction, *ISPRS J. Photogramm. Remote Sens.* 212 (2024) 181–192.
- [41] G. Ke, Q. Meng, T. Finley, T. Wang, W. Chen, W. Ma, Q. Ye, T.-Y. Liu, Lightgbm: A highly efficient gradient boosting decision tree, *Adv. Neural Inf. Process. Syst.* 30 (2017).
- [42] G. Logeswari, S. Bose, T. Anitha, An intrusion detection system for sdn using machine learning, *Intell. Autom. Soft Comput.* 35 (1) (2023) 867–880.
- [43] S. Lundberg, A unified approach to interpreting model predictions, 2017, arXiv preprint arXiv:1705.07874.
- [44] Z. Wu, R. Qiao, S. Zhao, X. Liu, S. Gao, Z. Liu, X. Ao, S. Zhou, Z. Wang, Q. Jiang, Nonlinear forces in urban thermal environment using Bayesian optimization-based ensemble learning, *Sci. Total Environ.* 838 (2022) 156348.
- [45] S. Alavipanah, J. Schreyer, D. Haase, T. Lakes, S. Qureshi, The effect of multi-dimensional indicators on urban thermal conditions, *J. Clean. Prod.* 177 (2018) 115–123.
- [46] M. Deng, W. Yang, C. Chen, Z. Wu, Y. Liu, C. Xiang, Street-level solar radiation mapping and patterns profiling using Baidu Street View images, *Sustain. Cities Soc.* 75 (2021) 103289.
- [47] S. Grimmond, Urbanization and global environmental change: local effects of urban warming, *Geogr. J.* 173 (1) (2007) 83–88.
- [48] X. Yang, Y. Li, The impact of building density and building height heterogeneity on average urban albedo and street surface temperature, *Build. Environ.* 90 (2015) 146–156.
- [49] C. Yin, M. Yuan, Y. Lu, Y. Huang, Y. Liu, Effects of urban form on the urban heat island effect based on spatial regression model, *Sci. Total Environ.* 634 (2018) 696–704.
- [50] A. Sekertekin, E. Zadbagher, Simulation of future land surface temperature distribution and evaluating surface urban heat island based on impervious surface area, *Ecol. Indic.* 122 (2021) 107230.
- [51] S. Arshad, S.R. Ahmad, S. Abbas, A. Asharf, N.A. Siddiqui, Z. ul Islam, Quantifying the contribution of diminishing green spaces and urban sprawl to urban heat island effect in a rapidly urbanizing metropolitan city of Pakistan, *Land Use Policy* 113 (2022) 105874.
- [52] D. Hidalgo-García, J. Arco-Díaz, Modeling the Surface Urban Heat Island (SUHI) to study of its relationship with variations in the thermal field and with the indices of land use in the metropolitan area of Granada (Spain), *Sustain. Cities Soc.* 87 (2022) 104166.
- [53] S. Gao, Q. Zhan, C. Yang, H. Liu, The diversified impacts of urban morphology on land surface temperature among urban functional zones, *Int. J. Environ. Res. Public Heal.* 17 (24) (2020) 9578.
- [54] N. Zhang, J. Zhang, W. Chen, J. Su, Block-based variations in the impact of characteristics of urban functional zones on the urban heat island effect: A case study of Beijing, *Sustain. Cities Soc.* 76 (2022) 103529.
- [55] S. Zhou, T. Shi, S. Li, Y. Dong, J. Sun, The Impact of Urban Morphology on Multiple Ecological Effects: Coupling Relationships and Collaborative Optimization Strategies, in: *Building Simulation*, vol. 16, Springer, 2023, pp. 1539–1557.
- [56] S. Du, Y. Wu, L. Guo, D. Fan, W. Sun, How does the 2D/3D urban morphology affect the urban heat island across urban functional zones? A case study of Beijing, China, *ISPRS Int. J. Geo-Inf.* 13 (4) (2024) 120.
- [57] K. Yu, Y. Chen, D. Wang, Z. Chen, A. Gong, J. Li, Study of the seasonal effect of building shadows on urban land surface temperatures based on remote sensing data, *Remote. Sens.* 11 (5) (2019) 497.
- [58] Y. Liu, Y. Xu, F. Zhang, W. Shu, A preliminary study on the influence of Beijing urban spatial morphology on near-surface wind speed, *Urban Clim.* 34 (2020) 100703.
- [59] D. Han, T. Zhang, Y. Qin, Y. Tan, J. Liu, A comparative review on the mitigation strategies of urban heat island (UHI): a pathway for sustainable urban development, *Clim. Dev.* 15 (5) (2023) 379–403.